RSC Advances

This is an *Accepted Manuscript*, which has been through the Royal Society of Chemistry peer review process and has been accepted for publication.

Accepted Manuscripts are published online shortly after acceptance, before technical editing, formatting and proof reading. Using this free service, authors can make their results available to the community, in citable form, before we publish the edited article. This *Accepted Manuscript* will be replaced by the edited, formatted and paginated article as soon as this is available.

You can find more information about *Accepted Manuscripts* in the Information for Authors.

Please note that technical editing may introduce minor changes to the text and/or graphics, which may alter content. The journal's standard Terms & Conditions and the Ethical guidelines still apply. In no event shall the Royal Society of Chemistry be held responsible for any errors or omissions in this *Accepted Manuscript* or any consequences arising from the use of any information it contains.

ROYAL SOCIETY OF CHEMISTRY

www.rsc.org/advances

Boron nitride nanotubes biocompatibility has been evaluated on rat mesenchymal stem cells, in terms of proliferation and differentiation.

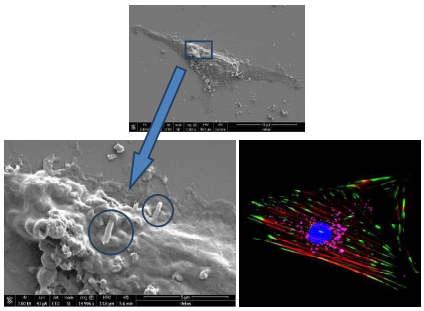

RSC Advances Accepted Manuscript

Journal Name

RSCPublishing

ARTICLE

Evaluation of effects of gum Arabic functionalized boron nitride nanotubes on differentiation of rat mesenchymal stem cells

Cite this: DOI: 10.1039/xoxxoooooox

Received ooth January 2012,
Accepted ooth January 2012

DOI: 10.1039/xoxxoooooox

www.rsc.org/

Tiago H. Ferreira[a], Antonella Rocca[b,c], Attilio Marino[b,c], Virgilio Mattoli[b], Edesia M.B. Sousa[a], Gianni Ciofani[b*]

[a]SENAN, Centro de Desenvolvimento da Tecnologia Nuclear, CDTN/CNEN, Av. Presidente Antônio Carlos 6627, 30270-901 Belo Horizonte, Brazil

[b]Center for Micro-BioRobotics @SSSA, Instituto Italiano di Tecnologia, Viale Rinaldo Piaggio 34, 56025 Pontedera (Pisa), Italy

[c]The BioRobotics Institute, Scuola Superiore Sant'Anna, Viale Rinaldo Piaggio 34, 56025 Pontedera (Pisa), Italy

*** Corresponding author**

E-mail: gianni.ciofani@iit.it

Tel.: +39 050883019

Fax: +39 050883497

Nanostructured materials have been widely investigated envisaging biomedical applications, in particular with the aim of selectively carrying drugs or molecules of interest to a target tissue or organ. In this context, boron nitride nanotubes (BNNTs) functionalized with specific moieties have demonstrated to be useful candidates for the delivery of proteins, drugs, and also nucleic acids. In this study, the influence of gum Arabic functionalized BNNTs was evaluated on the differentiation process of mesenchymal stem cells. The nanotubes have been characterized by transmission electron microscopy, scanning electron microscopy, Fourier transform infrared spectroscopy, Raman spectroscopy, and dynamic light scattering. *In vitro* assays on mesenchymal stem cells were performed to evaluate their cytocompatibility in terms of cell viability and metabolic activity. Interactions cells/nanoparticles were further investigated through the analysis of the cytoskeleton conformation. Finally, the differentiation of mesenchymal stem cells into adipocytes and osteocytes, treated with safe doses of BNNTs, was assessed both at gene and phenotype level.

RSC Advances Accepted Manuscript

Journal Name RSCPublishing

ARTICLE

1. Introduction

Nanostructured materials have gained increasing interest for biomedical applications, in particular with the aim of selectively carrying drugs or molecules of interest towards a desired tissue or organ.[1] Nanoparticles own the ability to penetrate through very small capillaries, and pass through biologic membranes fostering different cell functions.[2]

In the field of stem cell biology, great advances have been achieved with the development of innovative platforms based on nanomaterials.[3] As a consequence, the influence of nanoparticles in the processes of self-renewal and differentiation of stem cells has been extensively studied. Among different classes of nanomaterials, carbon-based materials,[4, 5] inorganic nanoparticles based on metal oxides,[6, 7] metals[8, 9] and quantum dots[10, 11] are worth to be mentioned.

Mesenchymal stem cells (MSCs) have self-renewal capacity and known ability to differentiate into various phenotypes of mesenchymal origin.[12] The development of stem cell-based therapy is very important in regenerative medicine, focusing mainly on the process of localization, proliferation, differentiation, and migration of the cells to the tissue to be repaired.[8] In this context, boron nitride nanotubes (BNNTs) functionalized with specific moieties can be useful nanovectors and could influence the differentiation process because of their peculiar physical/chemical properties.[13] BNNTs have demonstrated interesting characteristics exploitable in the biomedical field, thanks to their chemical inertness and cytocompatibility.[14] It has been shown, as an example, that BNNTs can be internalized by cells through an energy-dependent process,[15] and also efficiently deliver DNA with no apparent toxicity.[16]

To improve the possibilities of application, it is highly desirable to functionalize BNNTs with bioactive, yet biocompatible agents. In this study, BNNTs have been functionalized with gum Arabic (GA), a natural polysaccharide with good water solubility and well-recognized biocompatibility, already efficiently exploited for BNNT disentanglement.[17] After an extensive characterization of the obtained GA-BNNTs, their effects on MSC proliferation and differentiation have been evaluated, confirming once more biosafety of BNNTs and their ability to foster peculiar functions in a biological context.

2. Methods

2.1 Preparation and characterization of GA-BNNTs

Boron nitride nanotubes were prepared through a chemical synthesis based on a CVD (chemical vapor deposition) method, as described in a previous work.[18] Ammonium nitrate NH_4NO_3 (95% w/w), amorphous boron (97% w/w), and hematite (95% w/w and particle size less than 50 nm) were mixed at a molar ratio of 15:15:1, respectively, and heat-treated in a tubular furnace. The final product underwent a purification procedure with HCl (3 M) at 90 °C for 10 min, before being collected by filtration and dried at 40°C. Dispersive X-ray spectroscopy (EDX, Bruker), performed on a scanning electron microscope (SEM Helios NanoLab 600i, FEI), provided a composition characterized by N (45.6 ± 6.4%), B (37.4 ± 6.2%), C (9.8 ± 2.0%), O (6.5 ± 1.3%), and traces of Na, Cl and Ca (collectively about 0.8 ± 0.1%).[19]

Synthesized nanotubes have been characterized though a transmission electron microscopy (TEM) on a Tecnai G2-20-FEI 2006 microscope, with an acceleration voltage of 200 kV.

Analysis of Raman scattering was carried out in a Horiba Jobin Yvon device, model IHR 550, equipped with a monochromator, a confocal microscope (Olympus BH-2), and a CCD detector. The scattering was stimulated using a 2.4 eV laser (λ = 514.25 nm) with an objective lens of 50x. The accumulation time was 5x7 s, at 2.67 mW. Spectrum was collected in a wavelength range from 1000 to 1700 cm^{-1}.

BNNTs were functionalized with gum Arabic (GA) by a non-covalent coating. In a polystyrene tube, 10 mg of BNNTs ha been dispersed in 10 mL of ultrapure MilliQ® water (Millipore) and sonicated for 1 h. Then, 10 mg of GA was added and th sonication process was kept overnight. The functionalized product (GA-BNNT) was obtained as a dispersion with concentration of 1 mg/mL.

GA-BNNTs were characterized by Fourier transform infrared (FTIR) spectroscopy with a Thermo Scientific Nicolet 670 spectrophotometer, in the range 4000-600 cm^{-1}, with 64 scans and 4 cm^{-1} of resolution.

The morphological characteristics of functionalized BNNTs were studied using scanning electron microscopy (SEM), performed with a Carl Zeiss Sigma VP microscope. The sample was prepared by placing a drop of diluted GA-BNNT dispersion on a silicon wafer substrate, and allowing the substrate to air-dry before gold-sputtering.

Particle size distribution was assessed through dynamic light scattering with a Zeta-Sizer Nanoseries Zs (Malver Instruments).

2.2 Mesenchymal stem cell cultures and cytocompatibility assays

Rat mesenchymal stem cells (PT-2505) purchased from Lonza were maintained in low-glucose Dulbecco's modified Eagle's medium (DMEM) with 10% fetal bovine serum, 100 IU/ml penicillin, 100 µg/ml streptomycin and 2 mM L-glutamine at 37 °C. The atmosphere was kept at 95% air/5% CO_2, with 100% of humidity.

Viability tests were performed by using WST-1 metabolic assay (2-(4-iodophenyl)-3-(4-nitophenyl)-5-(2,4-disulfophenyl)-2H-tetrazoilium monosodium salt, provided in a pre-mix electro-coupling solution from BioVision). After trypsinization, cells were counted with a hemocytometer and seeded at a density of 5000/cm^2 in 96-well plate wells (n = 6). After cell adhesion (about 12 h since seeding) cells were incubated with 0, 5, 10, 20, 50, and 100 µg/ml of GA-BNNTs for 1, 3 and 7 days. At each time-point, cultures were treated with 100 µl of culture medium supplemented with 10 µl of the pre-mix solution f further 2 h. Absorbance at 450 nm was read by using a microplate reader (Victor3, Perkin Elmer).

Cell viability after 7 days of BNNT incubation was furthe assessed with the Live/Dead® viability/cytotoxicity kit (Molecular Probes), able to fluorescently label viable cells in green (thanks to the conversion of calcein-AM into calcein b

RSC Advances Accepted Manuscript

living cells) and necrotic cells in red (thanks to the ability of ethidium homodimer-1 to stain nuclei of cells with compromised membrane). Treated cultures were observed under an inverted fluorescence microscope (Eclipse TI, Nikon) equipped with a cooled CCD camera (DS-5MC USB2).

Cytoskeleton / focal adhesion staining kit (Millipore) was used for actin filaments and vinculin distribution analysis. Briefly, after GA-BNNT treatment, cells were fixed using a 4% paraformaldehyde (Sigma) solution in PBS for 15 min at 4°C. Next, cells were treated with a 0.1% Triton X-100 (Sigma) solution in PBS for membrane permeabilization. Goat serum at 10 % in PBS was added and left for 45 min to allow saturation to occur, then incubation with the vinculin primary monoclonal antibody (diluted 1:100 in 10% goat serum) was carried out for 45 min. Finally, the incubation with a staining solution composed by a green fluorescent labeled secondary antibody (AP124F from Millipore, diluted 1:50 in 10% goat serum), 100 µM TRITC-phalloidin for f-actin staining, and 1 µM DAPI for nucleus staining was performed for 30 min.

Images were also acquired with a confocal laser scanning microscope (C2s, Nikon), and treated with NIS professional software. BNNTs were observed by using an excitation wavelength of 642 nm, and collecting the fluorescence emission from 670 nm to 750 nm.

For scanning electron microscopy, samples incubated with 20 µg/mL of GA-BNNTs were fixed with two sequential incubations with a 4% paraformaldehyde solution (30 min at 4 °C) and with a 2.5% glutaraldehyde solution (30 min at 4 °C). Samples were thereafter dehydrated through an ethanol gradient (0, 25, 50, 75 and 100%) treatment, dried overnight and gold-sputtered before SEM observation.

2.3 Mesenchymal stem cell differentiation

In order to assess MSC differentiation into adipocytes, cells were cultured in 24-well plate chambers. They were allowed to reach confluence in standard culture medium, which was later replaced with adipogenic induction medium constituted by high-glucose DMEM, 100 U/ml penicillin, 5 µg/ml insulin, 200 mM L-glutamine, 10 % FBS, 1 µM dexamethasone, 20 µM indomethacin, and 500 µM 3-isobuty-l-methyl-xanthine. The concentrations of GA-BNNTs added to culture medium were 0, 10 or 20 µg/mL. Differentiation was assessed after 7 days since differentiation induction through the AdipoRed™ (Lonza) staining, that enables the quantification of intracellular lipid droplet accumulation. After being washed with PBS, cells were incubated at room temperature for 10 min with 1 mL of PBS and 30 µL of reagent. Cultures were observed with fluorescence microscopy.

For the differentiation of MSC in osteocytes, collagen coated 24-well plate chambers were seeded with MSCs and allowed to reach confluence. Thereafter, for osteogenic differentiation, medium was supplemented with 100 nM dexamethasone, 200 mM L-glutamine, 200 µM ascorbate, 10% FBS and 10 mM β-glycerophosphate. Concentrations of 0, 10 or 20 µg/mL of GA-BNNTs were added to the culture medium and cells incubated for 21 days. Alizarin Red assay was performed to evaluate the osteogenesis of MSCs thanks to the ability of this dye to specifically binds the calcium portion of the bone-like nodules deposited in the cultures. Cells were washed with PBS and fixed with 4% paraphormaldeyde (20 min at 4 ºC) and incubated with 500 µL of the staining reagent at room temperature for 30 min. To remove excess reagent, cells were washed three times (5 min each) with water and thereafter observed through bright-field microscopy.

MSC differentiation status was finally investigated throughout quantitative real-time reverse-transcription polymerase chain reaction (qPCR) to evaluate the expression of some constitutive osteoblastic and adipogenic markers at gene level on cultures differentiated in the presence of 0, 10, and 20 µg/mL of GA-BNNTs. Total RNA was extracted from cell cultures by using the High Pure RNA Isolation kit (Roche) according to the manufacturer's protocol. Extracted RNA concentration was measured at 260 nm with a spectrophotometer (Lambda 45, Perkin Elmer). RNA (100 ng) was reverse-transcribed into cDNA with 4 µl of iScriptTM Reverse Transcription Supermix (5X, Bio-Rad) in a total volume of 20 µL. After an initial incubation at 25°C for 5 min, the program included an incubation at 42°C for 45 min and at 48°C for 15 min; finally the reaction was inactivated at 85°C for 5 min. Quantitative RT-PCR was performed with a CFX Connect™ Real-Time PCR Detection System (Bio-Rad). The obtained cDNA was diluted with ultra-pure water 1:10, and 5 µl of this cDNA was mixed with 1 µl of specific forward and reverse primers (8 µM), 4 µl of MilliQ® and 10 µl of SsoAdvancedTM SYBR®Green Supermix (Bio-Rad). Primer sequences of the examined genes are reported in Tables 1-3. The procedure applied was the following: one cycle of 30 s at 98°C for enzyme activation, 40 cycles at 98 °C for 3 s and 60 °C for 15 s, a temperature ramp from 65 °C to 95 °C, with 0.5 °C/s increments, to discard unspecific products. Ribosomal protein L19 (RPL19: F – CATGGATGAGGAGAATGAGGATT, R – CCCACACTTCCTCTCTCCT) was used as reference gene to normalize the results of the transcription levels. All tests were performed in triplicate and comprise "no template" sample as control of the reaction. To calculate differences in gene expression level, we adopted the $\Delta\Delta C_t$ formula,[20, 21] where ΔC_t value is the difference between the cycle threshold (C_t) of target and housekeeping gene.

2.4 Statistical analysis

Results are presented as the mean for each group ± the standard deviation. Statistical evaluation of the data was performed using analysis of variance (ANOVA), followed by Bonferroni's *post-hoc* test, and $p < 0.05$ was considered to be statistically significant. WST-1 tests were performed in esaplicate and the remaining assays were performed in triplicate. In all cases, three independent experiments were carried out.

3. Results and discussion

3.1 BNNT characterization

Figures 1a-b show representative TEM images of the BNNTs used in this work, both at low (a) and high magnification (b). In Figure 1b we can appreciate the hollow inner channel of the nanotube and its walls (about 30); the diameter is about 70 nm.

From the Raman spectrum showed in Figure 1c it is possible to observe the presence of a single peak at 1370 cm^{-1}, which is characteristic of the tangential vibration mode of BNNTs, as described in the literature.[22] From this analysis, it has been possible to confirm that this sample presents boron nitride structured in the nanotube form, even in the presence of a relatively high background.[23]

SEM imaging of GA-BNNTs (Figure 2a) revealed the presence of nanotube measuring about 150 nm in diameter, a greater value with respect to that one evidenced by TEM, most probably because of the presence of a gum Arabic wrapping layer, and length up to 1 µm. This image is representative of a typical GA-BNNT sample, presenting uniform diameters and rough surfaces.

RSC Advances Accepted Manuscript

Through the dynamic light scattering the evaluation of average distribution size was performed, as reported in Figure 2b. The hydrodynamic diameter (D_H) distribution was measured up to two weeks since the preparation, and remained constant around 425 ± 25 nm, indicating a good stability of the obtained dispersion. From this value, the average nanotube length L corresponding to the experimental D_H was determined by exploiting following equation:

$$D_H = \frac{L}{\ln(\frac{L}{d}) + 0.32} \quad (1)$$

where d is the diameter of the nanotube (d = 150 nm), in agreement to the model described by Nair *et al.*[24] An average BNNT length of 0.9 µm, coherently with the SEM observations, has been obtained.

Figure 2c shows a comparative FTIR spectrum study of plain BNNTs (black), GA-BNNTs (red), and gum Arabic (blue). The most important feature displayed in the spectra is the strong asymmetric band centered at 1380 cm^{-1}, corresponding to the B-N stretch bond, together with a less intense band at 790 cm^{-1} ascribed to the B-N-B bond.[25] The sample functionalized with GA (blue) presents a band centered at 1030 cm^{-1} which can be ascribed to the aromatic ether group of the GA. These results confirm the presence of GA on the BNNTs.

3.2 Biological testing

Viability was investigated with the Live/Dead® viability/cytotoxicity kit. Through the obtained images (Figure 3a) it was possible to verify that no significant evidence of cell membrane damage was present following treatment of cells up to 100 µg/ml of GA-BNNTs. This result clearly demonstrates an optimal cell viability, which was found comparable to that of the control cultures. Figure 3b shows quantitative results of the WST-1 assay, performed after 1, 3 and 7 days of incubation with 0-100 µg/mL of GA-BNNTs. Until the third day of treatment, there was no significant difference between the tested concentrations when compared to the control, thus indicating an excellent metabolic activity. After seven days of treatment, it was observed a small decrement in the cell viability at all the tested concentrations, becoming significant ($p < 0.05$) for the 50 and 100 µg/mL doses.

Cells were treated with different concentrations of GA-BNNTs (0-50 µg/mL) to verify possible changes in cytoskeleton, caused by reorganization of actin and vinculin patterns (Figure 4). The staining of f-actin filaments with fluorescent phalloidin revealed a qualitative modification of the cytoskeleton conformation in the cells treated with 50 µg/mL. The BNNTs can be in fact internalized by cells,[26] and at higher concentrations this process is enhanced: this up-take modifies the cytoskeleton conformation and, consequently, the mechanical properties of the cells are expected to be affected[27]. A significant alteration in the pattern of cytoskeleton filaments is in fact supposed to affect the tension of the whole cell structure, according to the model of the tensegrity architecture.[28] Changes of cytoskeleton arrangement are moreover of particular importance if we consider their effects on stem cell proliferation and differentiation. It has been proven, in fact, as cytoskeleton conformation and tension play a key role in determining stem cell fate, by mechanically influencing several signaling pathways and, consequently, stem cell differentiation.[29] Cytoskeleton arrangement and conformation can be also exploited as "predictors" of stem cell fate, by using appropriate analysis of actin patterns, such as shapes, intensities, textures, and spatial distributions.[30]

SEM images of MSCs are presented in Figure 4a, before (left) and after (right) a 12 h incubation with 20 µg/mL of GA-BNNTs. The qualitative morphology of MSCs is comparable in both cultures, confirming no apparent negative effects caused by the presence of the nanostructures. Figure 5a moreover shows several nanotubes in contact with the cell membrane. At higher magnification, it is indeed possible to observe the exact moment when two nanotubes are being internalized by the cell. Evidence of cellular internalization of BNNTs is important to investigate their potential as nanovectors able to delivery molecules of interest inside the cells. Confocal microscopy was carried out on MSC cultures after incubation with GA-BNNTs. A representative confocal image is reported in Figure 5b. After 4 h of incubation with 20 µg/mL of GA-BNNTs the cells internalized the nanotubes at high extent, and this internalization process can be appreciated by the presence of highly fluorescent spots (pseudo-colored in pink) inside the cytoplasm. The cytoskeletal actin was labeled in red, vinculin in green. No evidence of BNNTs in the cell nuclei (stained in blue) could be observed.

The images of AdipoRed™ staining for assessing adipogenesis after 7 days of treatment with different concentrations of GA-BNNTs is shown in Figure 6a. Fatty lipid deposits, which are indicative of well-sustained adipogenesis, can be identified as green spots without apparent differences among samples treated with nanoparticles and control.

The qPCR results of samples induced to adipogenic differentiation for 7 days (Figure 6b) demonstrated a significant increase of the main adipogenesis markers in the presence of both 10 µg/ml of GA-BNNTs (*Cebpa* 1.5-fold, *Gpd1* 1.8-fold, *Lpl* 1.3-fold) and 20 µg/ml of GA-BNNTs (*Cebpa* 1.6-fold, *Gpd1* 2.5-folds, *Lpl* 1.4-fold, *Pparg* 1.2-fold), with respect to the control ($p < 0.05$). Furthermore, increasing the BNNT concentration leads to an increment the mRNA transcription of *Gpd1* (1.3-fold) when compared to the lowest dose of nanoparticles. *Pparg* is the key transcription factor of adipogenesis, and together with *Lpl*, which exerts a hydrolytic activity on triglycerides,[31] contribute to the early stage of adipocyte differentiation.[32] *Gpd1* and *Cebpa* are expressed by mature adipocytes: *Gpd1* converts dihydroxyacetone phosphate to glycerol-3-phosphate,[33] while *Cebpa* activates *Pparg* expression.[34] These data collectively indicate that GA-BNNTs promote adipocyte maturation, given our results that demonstrate an over-expression of adipogenesis markers (and especially of the late adipogenic genes) following GA-BNNT administration.

It is widely known that adipocyte maturation requires reactive oxygen species (ROS) production.[35] Previous studies demonstrated that BNNTs promote the ROS generation in cell some typologies of cells.[36] Therefore, our hypothesis is that BNNTs, by increasing oxidative stress, enhance the ability of MSCs to differentiate into adipocytes, at least at level of key gene transcription.

To test this hypothesis, we analyzed gene expression of two enzymes involved in the preservation of a favorable intracellular redox environment, namely *Gss* and *Gpx1*, which respectively encode glutathione synthetase and glutathione peroxidase 1. At the end of the adipogenesis experiments, we highlighted a significant up-regulation of both genes in cells differentiated in the presence of BNNTs (about 3-fold for both BNNT concentrations, $p < 0.05$, Figure 6c). The increment of the expression of these markers, coding for enzymes involved in the detoxification from ROS,[37] suggests a moderate oxidative stress induced by BNNTs, thus corroborating the hypothesis of

RSC Advances Accepted Manuscript

This journal is © The Royal Society of Chemistry 2012

an enhanced adypogenesis due to a higher level of ROS in the differentiating BNNT-treated cultures.

Concerning the osteogenesis evaluation, the images of Alizarin Red staining of MSCs after treatment with different concentrations of GA-BNNT are shown in Figure 7a. The results revealed no apparent changes in the calcium deposits among BNNT-treated and control samples.

qPCR was performed for the assessment of the transcription of genes involved in osteogenesis (Figure 7b). The analysis after 21 days of culture highlighted that BNNTs do not enhance the transcription of the main osteogenesis marker genes except for *Col1a1,* the predominant protein of bone matrix,[38] that was significant incremented both in presence of 10 µg/mL (1.4-fold) and 20 µg/mL (1.5-fold) of GA-BNNTs with respect to the control ($p < 0.01$).

Summarizing, gum Arabic coated BNNTs, dispersed in the growth medium, do not exert toxic effects on MSCs, enhance adipogenic differentiation of MSCs but do not significantly improve the osteogenesis process, this latter result being partially in contrast to the case of BNNTs used as "substrate" for stem cell differentiation,[39] most probably because of the main role played by the substrate stiffness during the differentiation process.

4. Conclusions

Biocompatibility of gum Arabic coated boron nitride nanotubes in rat mesenchymal stem cells was verified through several independent assays. Viability and proliferation were not affected by the treatment up to 20 µg/mL of GA-BNNTs. The internalization of nanotubes by MSCs was verified by SEM images and confirmed by confocal microscopy. The cytoskeleton arrangement was also studied, revealing a significant rearrangement of f-actin based structures, most probably due the up-take of the nanoparticles. Finally, BNNTs caused an enhancement of the differentiation process into adipocytes but not in osteocytes, as it can be observed from the qPCR data, that demonstrated an increment of the mRNA level of the major adipocyte differentiation marker genes.

Overall, we can conclude that once more BNNTs confirmed a satisfactory biocompatibility, also toward stem cells. Moreover, they demonstrated the ability to foster cellular phenotype by enhancing adipogenic differentiation. This "smart" property could be exploited to improve the MSC adipogenic differentiation in cell therapy approaches, although additional studies are necessary to further examine the complete maturation of MSCs toward adipocytes, and to understand the molecular mechanisms involved in the BNNT-enhanced adipogenesis.

Acknowledgements

The authors wish to thank FAPEMIG (*Fundação de Amparo a Pesquisa do Estado de Minas Gerais*), CNPQ (*Conselho Nacional de Desenvolvimento Científico e Tecnológico*), and CAPES (*Comissão Aperfeiçoamento de Pessoal de Nível Superior*) for their financial support.

Figure and Table captions

Figure 1. Low (a) and high (b) magnification TEM images of a typical BNNT; Raman spectrum of the BNNT sample (c).

Figure 2. GA-BNNT characterization: SEM image (a), hydrodynamic size distribution (b), FTIR spectra (c).

Figure 3. (a) Live/Dead® viability/cytotoxicity assay performed on MSC cultures treated for 7 days with increasing concentrations of GA-BNNTs (green: living cells, red: necrotic cells); (b) WST-1 metabolic assay on MSC cultures incubated for 1, 3 and 7 days with increasing concentrations of GA-BNNTs (* $p < 0.05$).

Figure 4. Staining of actin, vinculin and nuclei in MSCs treated with different concentrations of GA-BNNTs.

Figure 5. Scanning electron microscopy images of MSCs before and after a 12 h incubation with 20 µg/mL of GA-BNNTs, at low and high magnification (a); confocal image showing GA-BNNTs (in pink) up-taken by MSCs. Cytoskeletal actin is stained in red, vinculin in green, nuclei in blue.

Figure 6. Images of AdipoRed™ staining for assessing adipogenesis in MSCs after 7 days of treatment with different concentrations of GA-BNNTs (a); quantification of adipogenesis marker gene transcription after 7 days of differentiation (b): CCAAT/enhancer binding protein (C/EBP) alpha (*Cebpa*), glycerol-3-phosphate dehydrogenase 1 (*Gpd1*), lipoprotein lipase (*Lpl*), peroxisome proliferator-activated receptor gamma (*Pparg*); quantification of ROS-related gene transcription after 7 days of differentiation (c): glutathione peroxidase 1 (*Gpx1*), glutathione synthetase (*Gss*).

Figure 7. Images of Alizarin Red staining for assessing osteogenesis in the MSCs after 21 days treatment with different concentrations of GA-BNNTs (a); quantification of osteogenesis marker gene transcription after 21 days of differentiation (b): alkaline phosphatase (*Alpl*), type 1 alpha collagen (*Col1a1*), runt-related transcription factor 2 (*Runx2*), secreted phosphoprotein 1 (*Spp1*).

Table 1. Sequences of primers of osteogenesis markers.

Table 2. Sequences of primers of adipogenesis markers.

Table 3. Sequences of primers of ROS-related genes.

Notes and references

1. M. Goldberg, R. Langer and X. Jia, *J Biomater Sci Polym Ed*, 2007, **18**, 241-268.
2. A. O. El-Sadik, A. El-Ansary and S. M. Sabry, *Clin Pharmacol*, 2010, **2**, 9-16.
3. G. Ciofani, L. Ricotti, C. Canale, D. D'Alessandro, S. Berrettini, B. Mazzolai and V. Mattoli, *Colloids Surf B Biointerfaces*, 2013, **102**, 312-320.
4. E. Jan and N. A. Kotov, *Nano Lett*, 2007, **7**, 1123-1128.
5. E. W. Brunner, I. Jurewicz, E. Heister, A. Fahimi, C. Bo, R. P. Sear, P. J. Donovan and A. B. Dalton, *ACS Appl Mater Interfaces*, 2014, **6**, 2598-2603.
6. K. Fujioka, S. Hanada, Y. Inoue, K. Sato, K. Hirakuri, K. Shiraishi, F. Kanaya, K. Ikeda, R. Usui, K. Yamamoto, S. U. Kim and M. Manome, *Int J Mol Sci*, 2014, **15**, 11742-11759.
7. K. Corsi, F. Chellat, L. Yahia and J. C. Fernandes, *Biomaterials*, 2003, **24**, 1255-1264.
8. A. Heymer, D. Haddad, M. Weber, U. Gbureck, P. M. Jakob, J. Eulert and U. Noth, *Biomaterials*, 2008, **29**, 1473-1483.
9. X. Liu, W. He, Z. Fang, A. Kienzle and Q. Feng, *J Biomed Nanotechnol*, 2014, **10**, 1277-1285.

RSC Advances Accepted Manuscript

10. S. Danner, H. Benzin, T. Vollbrandt, J. Oder, A. Richter and C. Kruse, *Int J Cell Biol*, 2013, **918242**, 24.
11. B. S. Shah and J. J. Mao, *Methods Mol Biol*, 2011, **680**, 61-75.
12. K. Le Blanc, C. Tammik, K. Rosendahl, E. Zetterberg and O. Ringden, *Exp Hematol*, 2003, **31**, 890-896.
13. P. Kral, E. J. Mele and D. Tomanek, *Phys Rev Lett*, 2000, **85**, 1512-1515.
14. G. Ciofani, S. Danti, G. G. Genchi, B. Mazzolai and V. Mattoli, *Small*, 2013, **9**, 1672-1685.
15. G. Ciofani, V. Raffa, A. Menciassi and A. Cuschieri, *Biotechnol Bioeng*, 2008, **101**, 850-858.
16. X. Chen, P. Wu, M. Rousseas, D. Okawa, Z. Gartner, A. Zettl and C. R. Bertozzi, *J Am Chem Soc*, 2009, **131**, 890-891.
17. Z. Gao, C. Zhi, Y. Bando, D. Golberg, M. Komiyama and T. Serizawa, *RSC Advances*, 2012, **2**, 6200-6208.
18. P. R. O. S. T. H. Ferreira, R. G. Santos, E. M. B. Sousa *J Biomater Nanobiotechnol* 2011, **2**, 426-434.
19. T. H. Ferreira, A. Marino, A. Rocca, I. Liakos, S. Nitti, A. Athanassiou, V. Mattoli, B. Mazzolai, E. M. de Sousa and G. Ciofani, *Int J Pharm*, 2015, **481**, 56-63.
20. D.-H. Kim, H.-S. Jang, C.-D. Kim, D.-S. Cho, H.-S. Yang, H.-D. Kang, B.-K. Min and H.-R. Lee, *Nano Letters*, 2003, **3**, 863-865.
21. J. H. Schefe, K. E. Lehmann, I. R. Buschmann, T. Unger and H. Funke-Kaiser, *J Mol Med*, 2006, **84**, 901-910.
22. R. Arenal, A. C. Ferrari, S. Reich, L. Wirtz, J. Y. Mevellec, S. Lefrant, A. Rubio and A. Loiseau, *Nano Lett*, 2006, **6**, 1812-1816.
23. J. Zhao, H. Lui, D. I. McLean and H. Zeng, *Appl Spectrosc*, 2007, **61**, 1225-1232.
24. N. Nair, W. J. Kim, R. D. Braatz and M. S. Strano, *Langmuir*, 2008, **24**, 1790-1795.
25. M. Zheng, Y. Liu, Y. Gu and Z. Xu, *Sci. China Ser. B-Chem.*, 2008, **51**, 205-210.
26. G. Ciofani, L. Ricotti, S. Danti, S. Moscato, C. Nesti, D. D'Alessandro, D. Dinucci, F. Chiellini, A. Pietrabissa, M. Petrini and A. Menciassi, *Int J Nanomedicine*, 2010, **5**, 285-298.
27. T. Feng, E. Szabo, E. Dziak and M. Opas, *Stem Cell Rev*, 2010, **6**, 74-85.
28. D. E. Ingber, N. Wang and D. Stamenovic, *Rep Prog Phys*, 2014, **77**, 046603.
29. P. Muller, A. Langenbach, A. Kaminski and J. Rychly, *PLoS One*, 2013, **8**.
30. M. D. Treiser, E. H. Yang, S. Gordonov, D. M. Cohen, I. P. Androulakis, J. Kohn, C. S. Chen and P. V. Moghe, *Proc Natl Acad Sci U S A*, 2010, **107**, 610-615.
31. H. Wang and R. H. Eckel, *Am J Physiol Endocrinol Metab*, 2009, **297**, 24.
32. S. R. Farmer, *Int J Obes Relat Metab Disord*, 2005, **29**, S13-S16.
33. Z. A. Schiller, N. R. Schiele, J. K. Sims, K. Lee and C. K. Kuo, *Stem Cell Res Ther*, 2013, **4**.
34. E. D. Rosen, C. H. Hsu, X. Wang, S. Sakai, M. W. Freeman, F. J. Gonzalez and B. M. Spiegelman, *Genes Dev*, 2002, **16**, 22-26.
35. H. Urakawa, A. Katsuki, Y. Sumida, E. C. Gabazza, S. Murashima, K. Morioka, N. Maruyama, N. Kitagawa, T. Tanaka, Y. Hori, K. Nakatani, Y. Yano and Y. Adachi, *J Clin Endocrinol Metab*, 2003, **88**, 4673-4676.
36. T. H. Ferreira, D. C. Soares, L. M. Moreira, P. R. da Silva, R. G. dos Santos and E. M. de Sousa, *Mater Sci Eng C Mater Biol Appl*, 2013, **33**, 4616-4623.
37. P. Maher, *Antioxid Redox Signal*, 2006, **8**, 1941-1970.
38. T. Katagiri and N. Takahashi, *Oral Dis*, 2002, **8**, 147-159.
39. L. Pauksch, S. Hartmann, M. Rohnke, G. Szalay, V. Alt, R. Schnettler and K. S. Lips, *Acta Biomater*, 2014, **10**, 439-449.

RSC Advances Accepted Manuscript

This journal is © The Royal Society of Chemistry 20 2

Gene	Symbol gene	Sequence (5' – 3')
Collagen, type I, alpha 1	Col1a1	F – GCAAAGAAGACTTGGACTGT R – TTCTGCGTCTGGTGATACA
Alkaline phosphatase	Alpl	F – GCACAACATCAAGGACATCG R – CATCCAGTTCATATTCCACATCAG
Runt-related transcription factor 2	Runx2	F – CCCTGAACTCAGCACCAA R – AGGATTGTGTCTGCCTGG
Secreted phosphoprotein 1	Spp1	F – AGGTGATAGCTTGGCTTACG R – TGTGGCATCGGGATACTG

Table 1.

RSC Advances Accepted Manuscript

Gene	Symbol gene	Sequence (5' – 3')
Peroxisome proliferator-activated receptor gamma	Pparg	F – GACCCAATGGTTGCTGATTAC R – GGACGCAGGCTCTACTTT
Glycerol-3-phosphate dehydrogenase 1	Gpd1	F – AGTTCTGTGAGACGACCATT R – CACTGTGTCCACCTCTTGTA
CCAAT/enhancer binding protein (C/EBP), alpha	Cebpa	F – GATAAGAACAGCAACGAGTACC R – GTCAACTCCAACACCTTCTG
Lipoprotein lipase	Lpl	F – GCCCAGCAACATTATCCAG R – GGGGTAGTTAAATTCTTCCTCCA

Table 2.

RSC Advances Accepted Manuscript

This journal is © The Royal Society of Chemistry 2012

Gene	Symbol gene	Sequence (5' – 3')
Glutathione peroxidase 1	Gpx1	F – CATTGTTTGAGAAGTGCGAGGTG R – ACTGGGTGCTGGCAAGGC
Glutathione synthetase	Gss	F – CCAGCGTGCCATAGAGAAC R – CCCTTTCAGAGACATCTTCAAATC

Table 3.

RSC Advances Accepted Manuscript

Figure 1

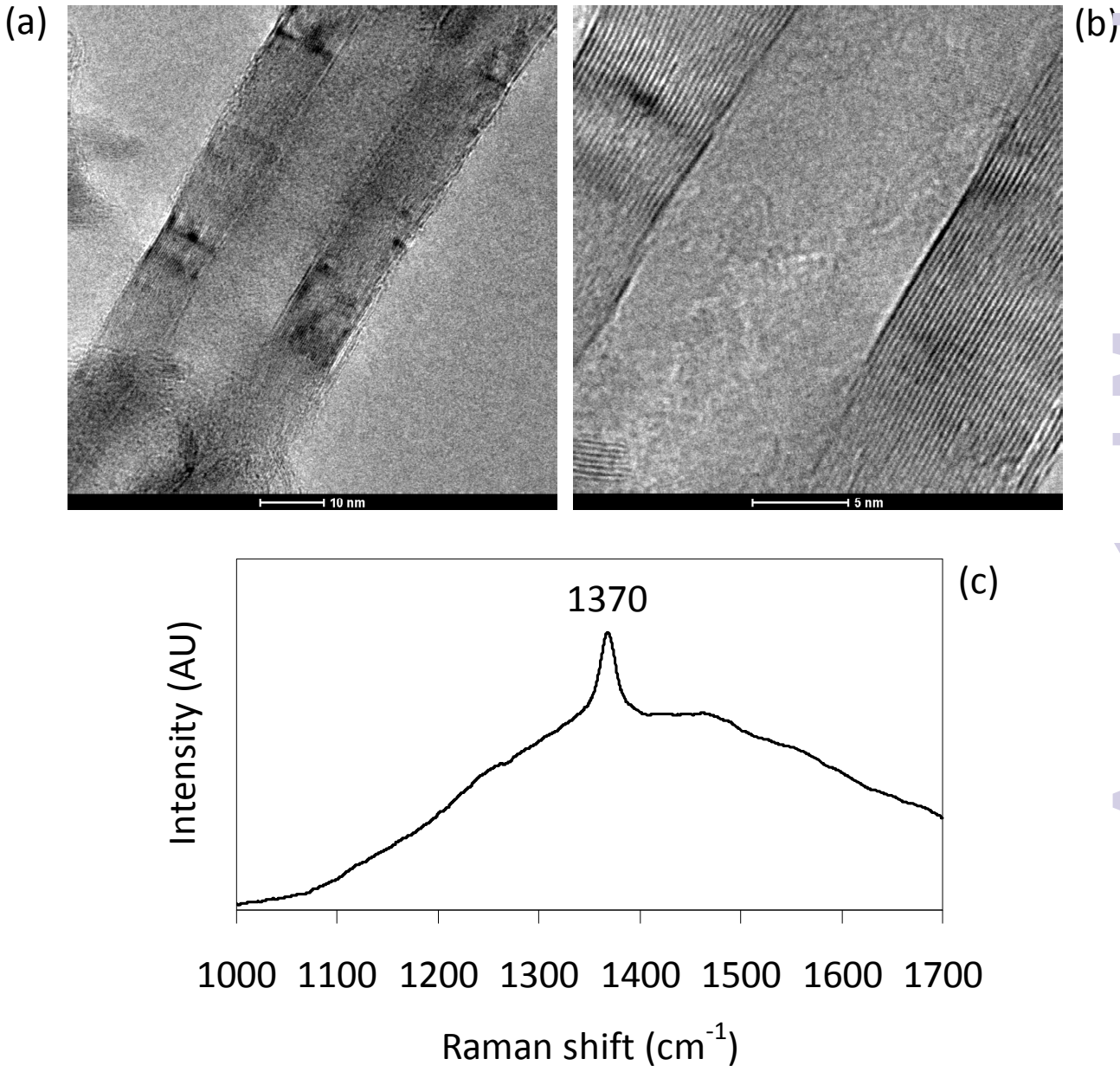

RSC Advances Accepted Manuscript

This journal is © The Royal Society of Chemistry 2012

Figure 2

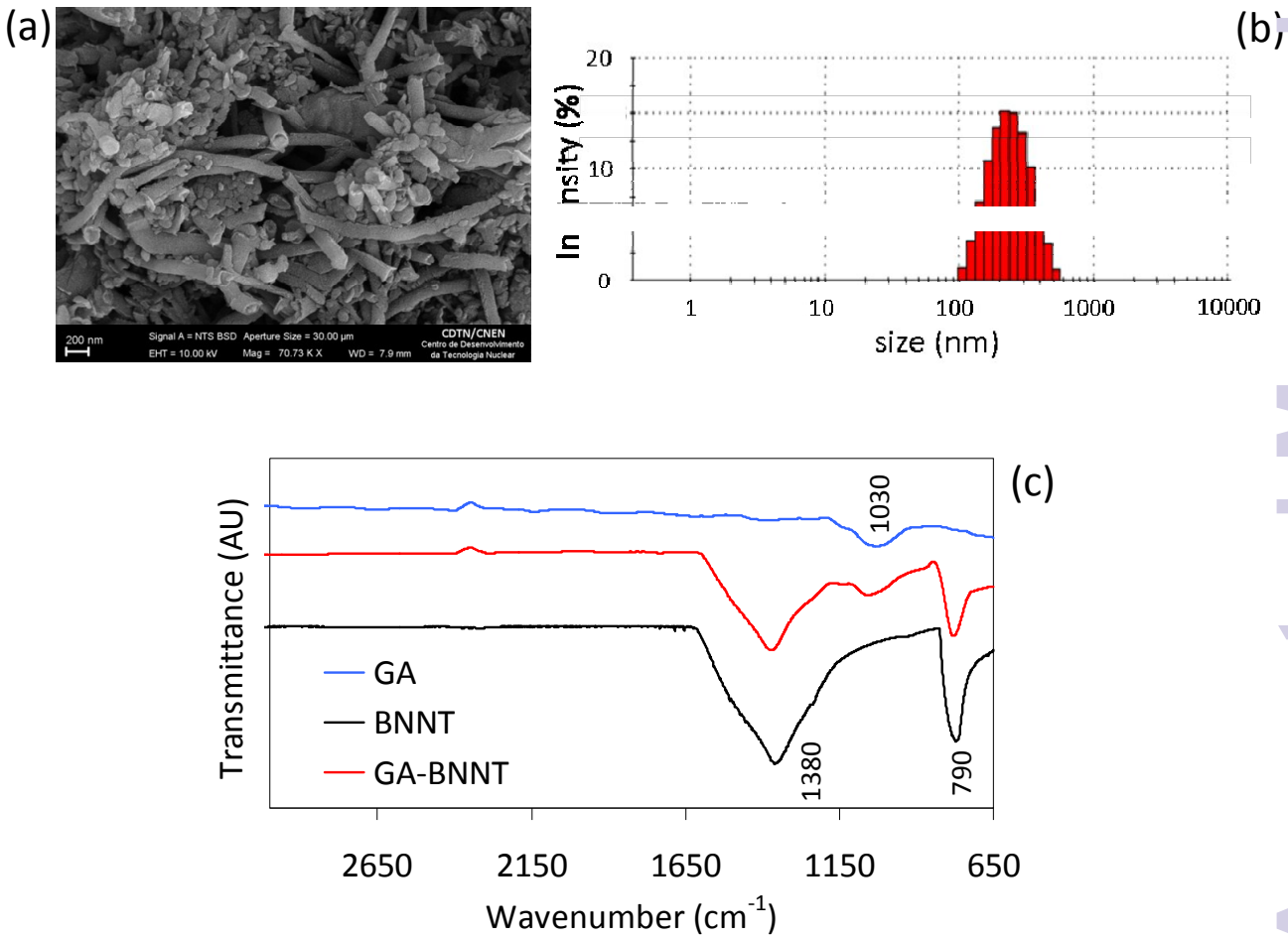

RSC Advances Accepted Manuscript

Figure 3

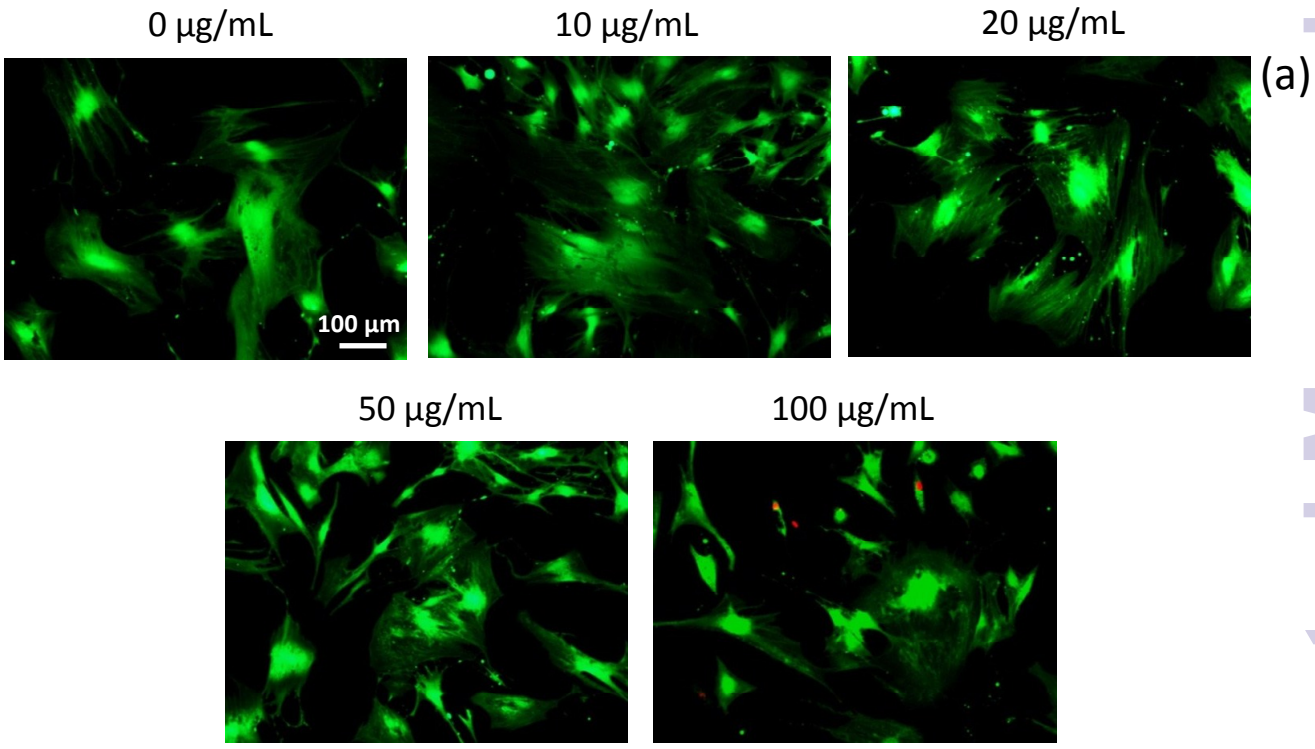

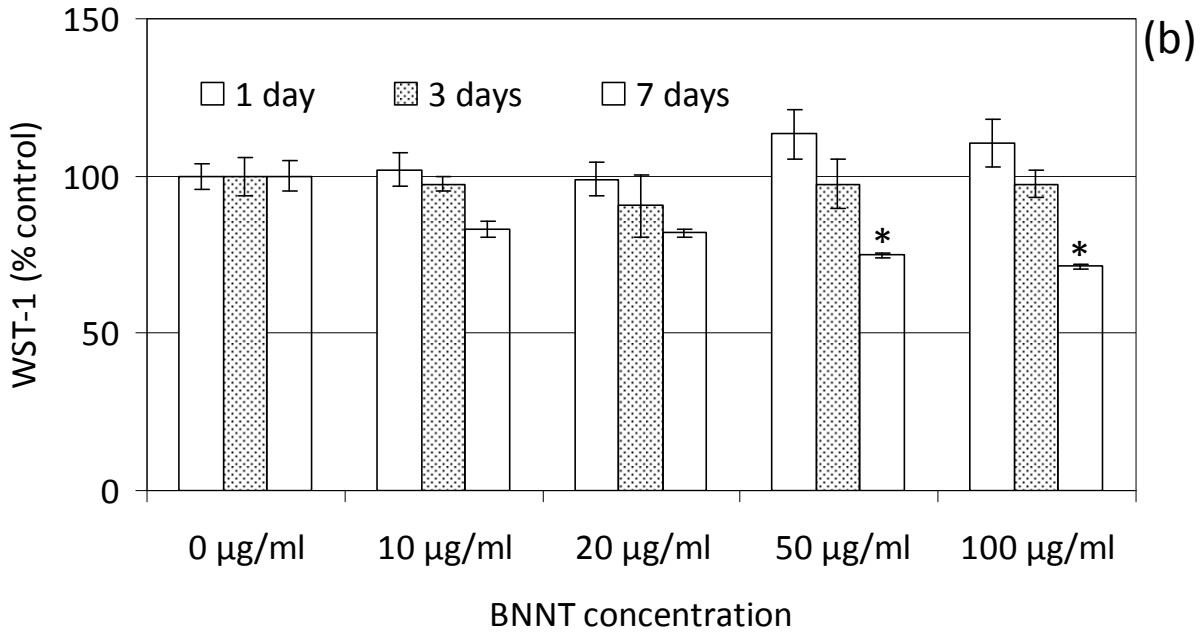

RSC Advances Accepted Manuscript

This journal is © The Royal Society of Chemistry 2012

Figure 4

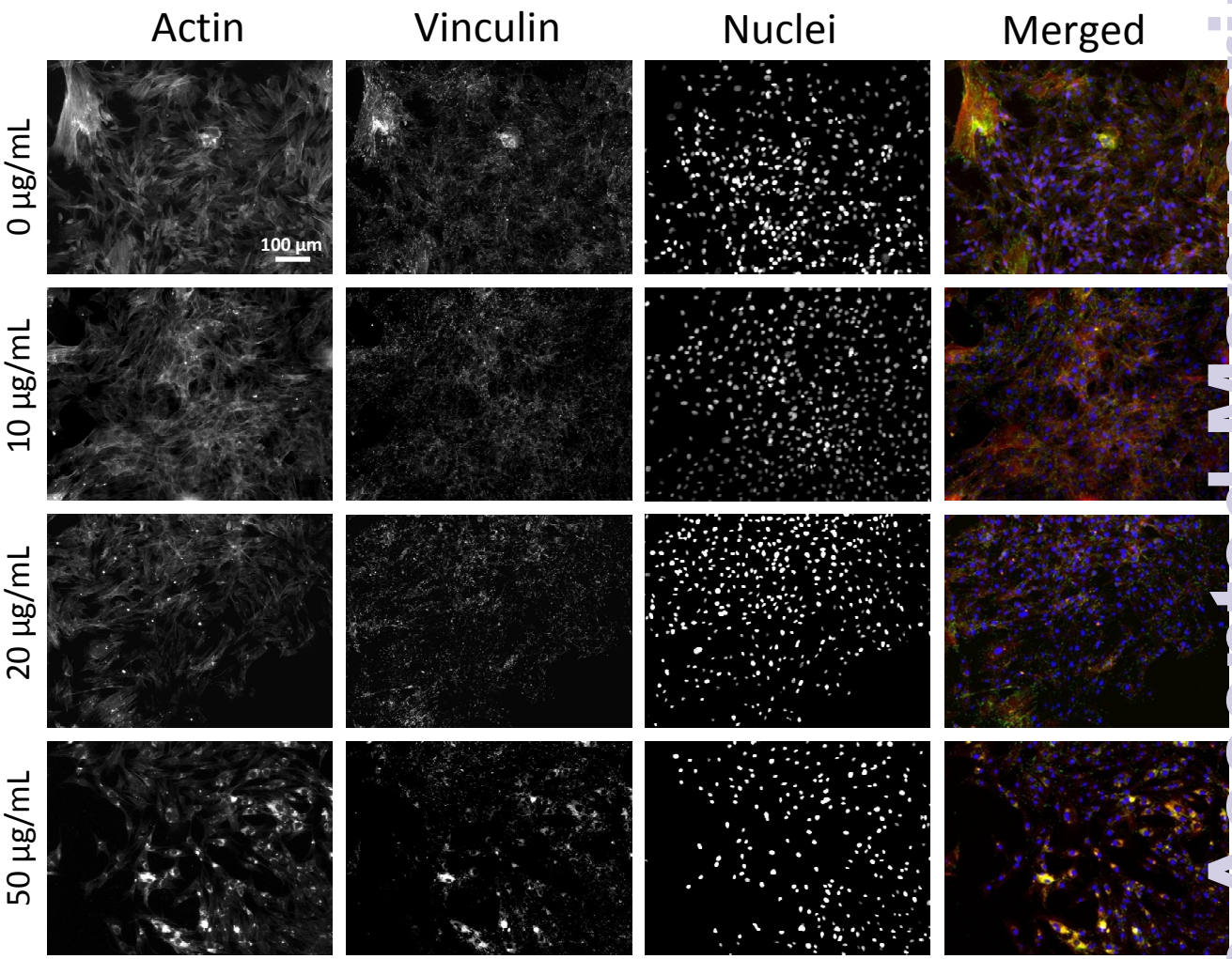

RSC Advances Accepted Manuscript

Figure 5

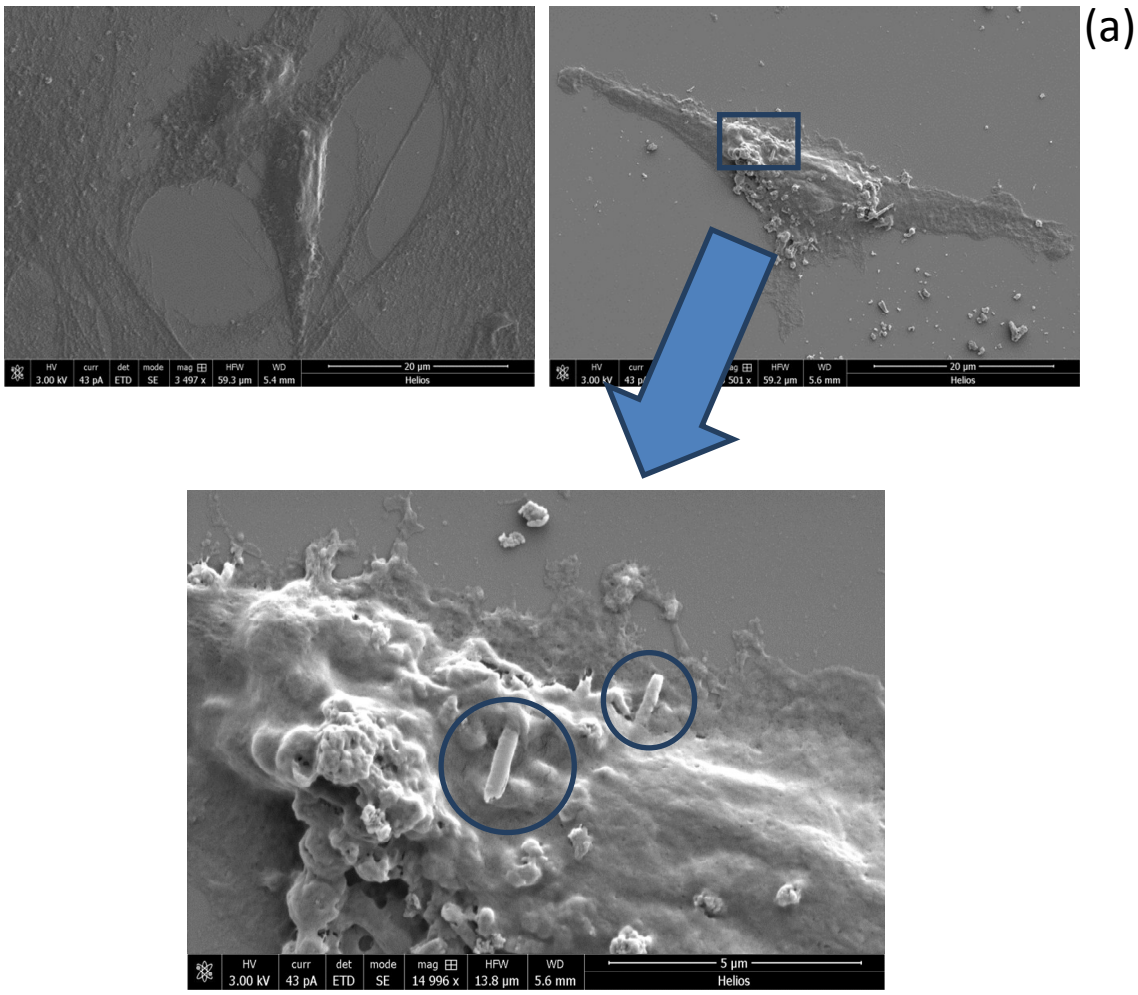

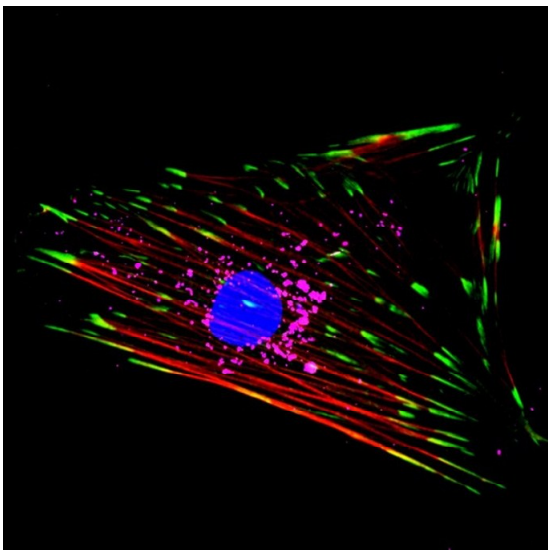

RSC Advances Accepted Manuscript

 This journal is © The Royal Society of Chemistry 2012

Figure 6

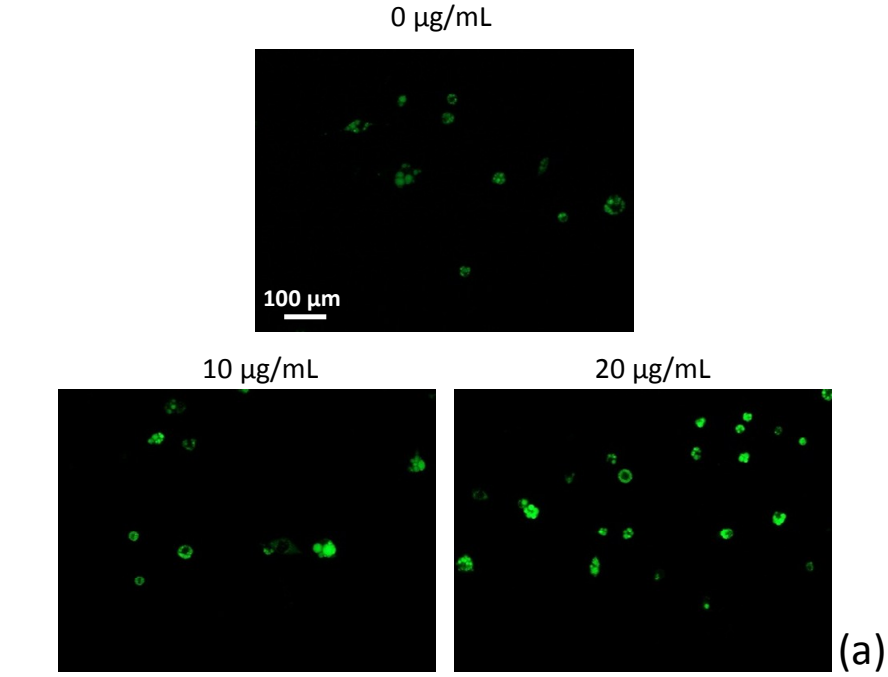

(a)

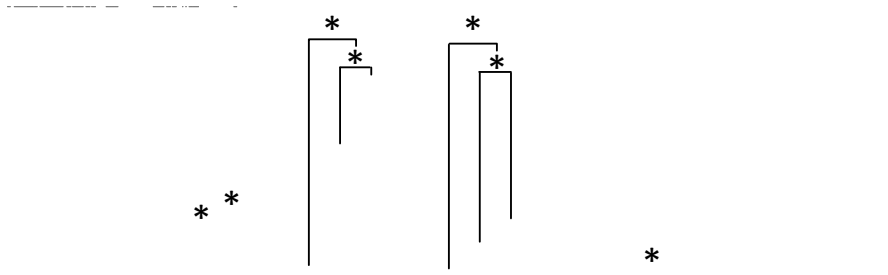

(b)

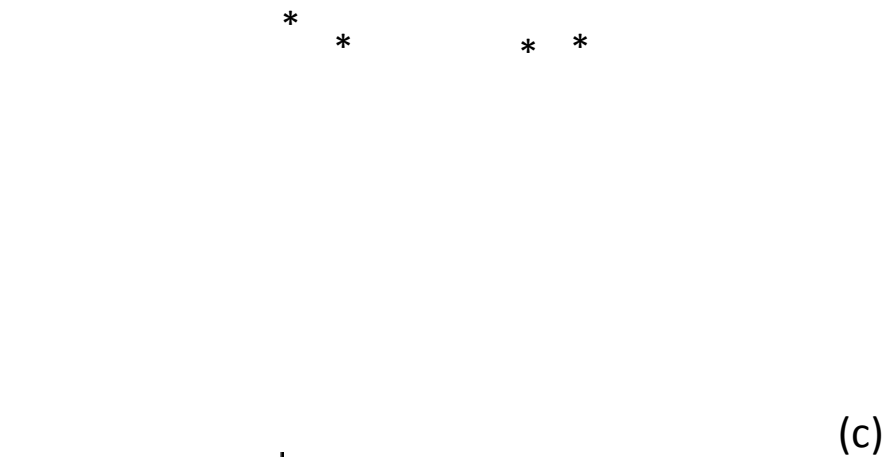

(c)

RSC Advances Accepted Manuscript

Figure 7

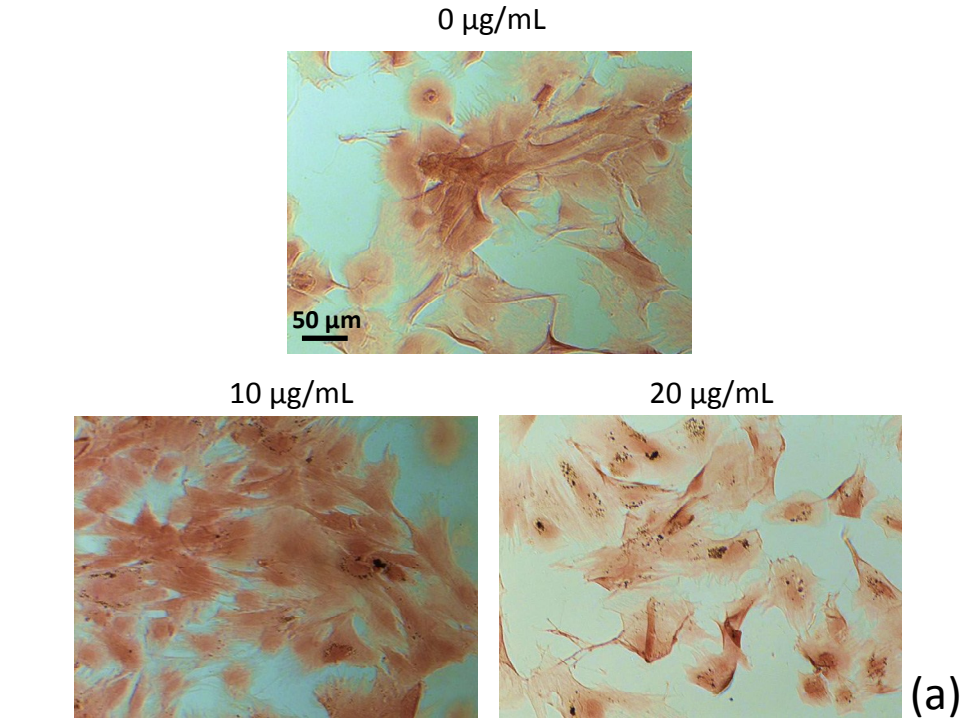

(a)

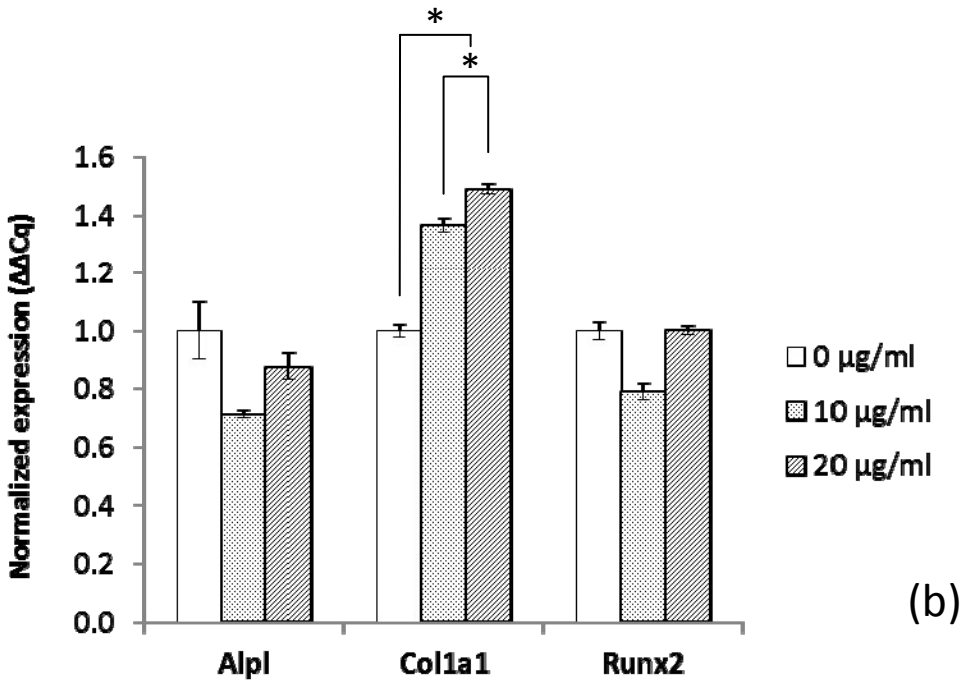

(b)

RSC Advances Accepted Manuscript

This journal is © The Royal Society of Chemistry 2012